2016-04-01

Video-based nearshore bathymetry estimation in macro-tidal environments

Bergsma, EWJ

http://hdl.handle.net/10026.1/6286

10.1016/j.margeo.2016.02.001
MARINE GEOLOGY
Elsevier BV

CPRG Paper9

Coastal Processes Research Group
School of Marine Science and Engineering
University of Plymouth
Drake Circus
PLYMOUTH, PL4 8AA
United Kingdom

Contact: daniel.conley@plymouth.ac.uk

The Coastal Processes Research Group is an internationally recognised group of researchers, specialising in field studies of coastal processes. We aim to be a leading contributor to the international research community seeking to understand and predict the behaviour of coastal and estuarine systems in support of appropriate management of coastal resources and activities.

Example Research Areas

- beach morphodynamics and nearshore sediment transport
- coastal erosion and storm impacts
- video monitoring of coastal systems
- coastal process modelling
- estuarine processes and evolution

Paper details

Citation	E.W.J. Bergsma, D.C. Conley, M.A. Davidson, T.J. O'Hare, Video-based nearshore bathymetry estimation in macro-tidal environments, Marine Geology, Volume 374, 1 April 2016, Pages 31-41, ISSN 0025-3227, http://dx.doi.org/10.1016/j.margeo.2016.02.001.		
Author(s)	E.W.J. Bergsma, D.C. Conley, M.A. Davidson, T.J. O'Hare		
Corresponding Author	erwin.bergsma@plymouth.ac.uk		
Funding bodies	UPDATE FIELD		
Paper URL publisher	http://www.sciencedirect.com/science/article/pii/S0025322716300159		
Date submitted	04 September 2015	**Last edit date**	08 October 2016

Video-Based Nearshore Bathymetry Estimation in Macro-Tidal Environments

E. W. J. Bergsma[a,1], D. C. Conley[a], M. A. Davidson[a], T. J. O'Hare[a]

[a]*School of Marine Science and Engineering, CPRG, Drake Circus, PL4 8AA, Devon, Plymouth, United Kingdom*

Abstract

Video-based depth inversion through the linear dispersion relation for free surface waves using the cross spectral correlation analysis, cBathy (Holman et al., 2013), is applied for the first time in a highly energetic macro-tidal environment in the South West of England at Porthtowan. This application of cBathy reveals two main issues: 1) inaccurate depth estimations on inter camera boundaries when multiple cameras are used and 2) significantly less accurate depth estimates over the whole domain during spring tide compared to neap tide (inaccuracies of around 35% of the local depths are found during spring tide). These two issues are not only important in macro-tidal environments: the camera boundary issue has been reported in numerous video-camera sites and the deviation in accuracy during tidal levels is a function of the tidal range in combination of the vertical camera position. To overcome the two issues, a camera boundary solution and a floating pixel solution (meaning moving pixels in a horizontal plane as function of the tidal elevation) are proposed here. With the modifications, cBathy is capable of

*Corresponding author

Email address: `erwin.bergsma@plymouth.ac.uk` (E. W. J. Bergsma)

estimating depths in the sub-tidal zone with an accuracy in the order of 10% of the local depth irrespective to the local tidal regime. However, for the very upper part of the beach face less accurate results are found due to the reduced validity of the linear dispersion relation in that region due to the non-linear behaviour of breaking waves and wave-current interactions. The improvements persist across all bathymetry survey campaigns at Porthtowan and when compared to other well known Argus video-system sites the importance of the floating pixels is apparent.
Keywords: depth-inversion, bathymetry estimation, video beach monitoring, macro-tidal, floating pixel solution, camera boundary solution

1. Introduction

Nearshore bathymetric information is crucial in understanding vulnerability of the near-shore coastal region to e.g. flood risk exposure, long- and short-term erosion/accretion and beach user safety. Extreme storms, for example, can lead to severe erosion of the inter- and sub-tidal domain of the near-shore zone. The impact on, and recovery rate of, the sub- and inter-tidal zone varies greatly depending on location (Masselink et al., 2015). Our comprehension of driving processes behind storm impact and recovery is limited and largely constrained by the quality of the available datasets (Coco et al., 2013). At present, there is a gap in understanding of the sub-tidal bar morphology and the interaction with the inter-tidal beach (Coco and Murray, 2007). Attempts to increase the knowledge of the nearshore zone are mostly based on intermittent bathymetry surveys or numerical models (Smit et al., 2008). The lack of high spatio-temporal resolution bathymetry data has been identified as a weakness in relation to setting initial conditions and for calibration of numerical models (Castelle et al., 2010). However, there are remote sensing techniques which have the potential to deliver this data (e.g. for the storm impact/recovery and interaction between sub- and inter-tidal) on a high spatio-temporal scale.

Remote sensing techniques for marine and coastal environments take many forms, from satellite-based systems estimating wave fields to SONAR for estimating depths in the ocean. Camera systems have been used to estimate depth and obtain beach slope information for over half a century starting in a hostile environment of enemy held beaches (Williams, 1946). The mathematical relation between wave length, wave velocity and water depth (e.g. the linear dispersion relation) was applied to aerial photographs taken in preparation of the World War II landings. More recently video imagery has been applied in a research context such as for measurement of swash excursions (Guza et al., 1984). Since the 1980s, several video based tools have been developed within the Argus-camera system framework (Holman and Stanley, 2007). Examples of these tools include the estimation of the crossshore position of sub-tidal sandbars by taking mean pixel intensities over a confined time space (Lippmann and Holman, 1990) and estimation of beach width by determining the shoreline position (Plant and Holman, 1997) which was later modified into an inter-tidal shoreline mapper (Aarninkhof et al., 2003). These tools in combination with the camera systems have given the research community and coastal-zone managers a relatively inexpensive way of investigating and monitoring shorelines worldwide.

Besides the qualitative crossshore position of the sub-tidal sandbars, much of the progress with video imagery over the last three decades has been focussed in the inter-tidal zone (Holman and Stanley, 2007). Although the inter-tidal area is important, Coastal Zone Management requires a more complete picture containing both the inter- and sub-tidal area as a basis for policy and decision making (Davidson et al., 2007). Accurate video camera-based sub- and inter-tidal depth information on a longer temporal scale provides data to enhance understanding about seasonal and inter-annual beach behaviour and storm recovery and gives the opportunity to adapt policies to local conditions. On a short time scale, up-to-date sub-tidal depth information is an important boundary condition for numerical models to improve the predictive capacity for short term computations such as the prediction of times and locations of highest risk for rip currents and hence provide lifeguards with accurate information to increase swimmer safety (Austin et al., 2013).

In the sub-tidal zone, remote sensing efforts have opened up the possibility to estimate depths accurately, primarily using video imagery or X-band radar. The most common approaches are depth-inversion methods, using the linear dispersion relation (Bell, 1999; Stockdon and Holman, 2000; Almar et al., 2008), non-linear depth inversion (Holland, 2001; Catálan and Haller, 2008) and extended Boussinesq equations (Misra et al., 2003). Another approach is the coupling of estimated dissipation rates with camera imagery and calculated rates with a numerical model (Aarninkhof et al., 2005). van Dongeren et al. (2008) brought these techniques (depth through dissipation rates and depth inversion) together in a data assimilation technique that combined the strong areas of both approaches. Wilson et al. (2010) shows that through data assimilation (wave and current measurements) using an ensemble Kalman filter, the accuracy of an updated, modelled, bathymetry can be enhanced. Remotely sensed (e.g. optical and radar) shore lines (Aarninkhof et al., 2005), wave celerity (Holman et al., 2013) and current fields (Chickadel, 2003) together can estimate morphology accurately through data assimilation without in-situ measurements (Birrien et al., 2013; Wilson et al., 2014). The focus in this study is on one of the parts of the data assimilation used in Wilson et al. (2014): sensing the wave celerity and, hence, the depth inversion technique (Holman et al., 2013).

Considering the first depth inversion technique mentioned above, the phase difference in pixel intensity between two pixels over a crossshore array gives a wave number from which the local depth can be found using the linear dispersion relation. This method of sensing the wave celerity between two pixels was limited in accuracy [O(10%)] on simple beaches (Holman and Stanley, 2007). A more robust method for determining the wave number in the coastal zone was recently developed using multiple pixels to fit a wave phase to an isolated frequency (Plant et al., 2008). The combination of the linear dispersion relation, wave phase fitting and a Kalman-like filter forms the latest, more robust version of cBathy (Holman et al., 2013). In Holman et al. (2013), the cBathy system was tested in the micro/meso tidal regimes at Duck, Oregon and Washington State in the United States. Testing of the performance of cBathy in a highly energetic macro-tidal environment (with more complex (3D) bathymetries) has been recently carried out (Bergsma et al., 2014) showing the effect of the tide on the accuracy in a macro tidal domain.

The wave-phase fitting of an isolated frequency requires accurate knowledge of the pixel positions in the real-world to prevent over or underestimation of the depth by fitting an incorrect phase ramp (Bergsma et al., 2014). In addition, inaccurate depth estimation is a common issue on the camera boundaries when multiple cameras are used. Accurate estimation of the phase ramp between two cameras is a challenge as the wave propagates through the camera boundaries from one to the other camera. The objective of this paper is to highlight tide and camera boundary related inaccuracies that are observed during the application of cBathy in a macro-tidal environment and, ultimately, present solutions to overcome both issues.

In the Methodology section the cBathy routines are explained in more depth and the study site, site specific cBathy settings and field data are presented. The Results section presents the results of the application of cBathy as well as a diagnosis of the inaccurate depth estimations on the camera boundary and inaccuracies caused by imprecise pixel locations. In the same section solutions are introduced and renewed depth estimations are presented. The Discussion places the findings in perspective and examines the generality of the findings to locations which are not necessarily macro tidal.

2. Methodology

2.1. cBathy

The principle behind cBathy (Holman et al., 2013) is that wave-modulated time varying pixel intensities can be used in combination with the linear dispersion relation for free surface waves to estimate a depth. Details of the process can be found in Holman et al. (2013) but the general concept is that the linear dispersion relation can be rearranged so that a depth (h) can be found as a function of the wave frequency (σ) and wave number (k) (1).

$$h = \frac{\tanh^{-1}\left(\frac{\sigma^2}{kg}\right)}{k} \tag{1}$$

Where g is the acceleration due to gravity. In order to apply (1) to estimate local depths, corresponding pairs of wave frequency and wave number values have to be determined. In cBathy, these parametres are estimated hourly using collection of pixel intensities recorded at 2Hz. The time varying pixel intensities are decomposed by applying a Fast Fourier Transform from which the subsequent Fourier coefficients are normalised.

To calculate depth at a specific location, a subset of these normalised Fourier coefficients surrounding the point of interest (x_m, y_m) are selected. Depending on the size of the sub-sampling domain (determined by smoothing scales L_x and L_y), a subset contains typically $40-50$ sub-samples with pixel coordinates x_p and y_p. The cross spectral density matrix (2) is computed for all possible pixel pairs in this subset and averaged across each frequency.

$$C_{i,j,f}^{OBS} = \left\langle \tilde{I}\left(x_i, y_i, f\right) \tilde{I}^*\left(x_j, y_j, f\right) \right\rangle = \gamma_{i,j,f} e^{i\phi_{i,j,f}} \tag{2}$$

Where $\tilde{I}$ represents the subset of the normalised Fourier coefficients and $\tilde{I}^*$ is the complex conjugate, γ represents the coherence and ϕ is the phase shift between pixel points. A selection (4 is the default) of the most coherent frequencies are identified (coherence is $\gamma_{i,j,f}$ in equation 2) and these are then used through the remainder of the analysis. For each selected frequency the cross-spectral density matrix is kept while the rest is neglected.

The cross-spectral density matrix essentially represents a noisy spatial (2D) wave pattern ($e^{i\phi_{i,j,f}}$) per selected frequency. Holman et al. (2013) included a complex empirical orthogonal function analysis in order to filter different physical components from the observed spatial pattern ($C_{i,j,f}^{OBS}$) per selected frequency. The inverse tangent of the dominant complex mode [1st complex eigenvector, $\upsilon_1 (x_p, y_p, f)$] is assumed to represent a wave train pattern which contains a phase spatial pattern $\upsilon_1' (x_p, y_p)$ at the frequency of interest (Wallace and Dickinson, 1972). This spatial pattern with known angular frequency can be represented by a wave phase as a function of the wave number k, wave angle α and phase shift Φ, as expressed in the right-hand side of (3). A Hanning filter is applied to the observed spatial pattern in order to give more importance to the values closer to the point of interest. A non-linear Least Squares fitting procedure is then applied to identify optimal values of k, α and Φ.

$$\underbrace{\upsilon_1' (x, y) = \tan^{-1} \left(\frac{Im\,(\upsilon_1 (x, y))}{Re\,(\upsilon_1 (x, y))} \right)}_{\text{Observed spatial phase pattern}} \cong \underbrace{k \cos(\alpha)\, x_p + k \sin(\alpha)\, y_p + \Phi}_{\text{Spatial wave phase for known frequency}} \tag{3}$$

The best-fit wave phase is determined for each selected frequency and results in a set of frequencies and corresponding wave numbers per point of interest where one wants to estimate a depth. This also means that multiple depth estimates are calculated at each point of interest. The set of depth estimates must be combined into a single depth, but simply averaging these depth estimates results in inaccuracies due to the non-linear character of the dispersion relation (1). Consequently a single depth is found yielding the best-fit relation between the selected frequencies and corresponding wave numbers to the linear dispersion relation. For each hourly dataset (or sampling period), this process is repeated throughout the field of view until depths have been estimated for a predetermined grid of points of interest (x_m, y_m).

Ultimately, the hourly estimated depths are combined through a Kalman Filter. The Kalman filter accounts for decay in faith in the depth estimate. Faith here means reliance upon the precision of the depth estimate that decreases over time due to the knowledge that morphological change will occur to a certain extent related to (in this case) changes in the wave height $[H_{m0}]$ only. When a new depth is estimated the filter updates the depth points with new estimates when the faith in the new estimate is considered greater than the faith in the previous estimate. The decay in faith in the depth estimate is captured in a process variability function Q (Holman et al., 2013), presented in (4), where a crossshore Gaussian distribution is constructed such that:

$$Q\left(x, H_{mo}\right) = C_Q H_{mo}^n \exp\left\{-\left[\frac{(x - x_0)}{\sigma_x}\right]^2\right\} \tag{4}$$

In this relation, C_Q represents a site specific constant, σ_x is the crossshore standard deviation of the allowable area of change and x_0 the crossshore position where the highest level of morphological variability is allowed. The highest level of temporal variability in the depth estimates is allowed where the value for Q is maximum and so the decay in faith of the previous depth estimates is largest. This implies in practice that x_0 should be defined by the user as the cross-shore location where one expects the greatest morphological change, following (4), with the result that estimates in that region are updated most readily.

2.2. Study site

The aim of this paper is to identify issues that occur when cBathy is applied in a macro tidal environment, namely Porthtowan in Cornwall in the South-West of England. At Porthtowan, the mean spring tidal range is 6.0 m and, in addition, highly energetic waves may be present. For the present study, an offshore wave buoy at Perranporth (see Figure 1, approximately 15 km North-East of Porthtowan in approximately 18 m water depth) was used to retrieve wave data, with the yearly averaged mean of the wave height being 1.6 m with an average direction of 281 °. During extreme events, wave heights of over 7 m have been recorded at this site (Masselink et al., 2015).

At Porthtowan beach, a single alongshore stretch of 2.5 km open beach at the foot of the rocky cliff appears during low tide reaching from Porthtowan to Chapel Porth. However, during mid to high tide the beaches are geologically constrained by the rocky cliffs creating 5 pocket beaches over the domain. The main and widest pocket beach (> 300 m) is the entrance at Porthtowan and the other pocket beach widths ranges from 100 to 250 m. The orientation of the beach at Porthtowan is W-NW, in correspondence with the dominant wave direction. Reflection of the waves on the rocky cliff during high tide is a potential complication for the accuracy of cBathy (not considered in this paper). Typically, the lower beach face exhibits a slope of approximately 0.015 whereas the upper beach face is steeper with a slope of 0.045. At the lower and upper part of the beach a grain size (D_{50}) of respectively 380 μm and 410 μm is found (Buscombe and Scott, 2008; Poate et al., 2014).

2.3. Implementation of cBathy at Porthtowan

cBathy requires model specific settings and boundary conditions such as domain settings, depth truncation, frequency domain and smoothing length scales. The camera system at Porthtowan is mounted on the Southern cliff and the cameras are looking alongshore in a Northerly direction, as shown in Figure 2a. Considering the spatial domain for the pixel intensity collections, the strategy used is to create the largest possible spatial domain stretching as far offshore as the method will allow. Practical limits to the offshore boundary are imposed by the depth controlled wave dispersion and the pixel resolution of the cameras. A reasonable offshore boundary for the domain is typically determined using the footprint of the pixel and occurring wave periods. The combination of wave periods and pixel footprint determines, at the same time, the spatial resolution (Δx and Δy) of the pixel collection (x_p and y_p). Following this procedure, the offshore boundary for the application of cBathy at Porthtowan was chosen to be 1.2 km offshore with Δx (crossshore) of 4 m and Δy (alongshore) of 10 m.

Points of interest on a (sub) grid are introduced (x_m, y_m) where the depth is estimated. The spacing between the gridded points for depth estimation is typically larger than the pixel intensity collection grid because for every depth estimate a set of sub-sampled pixel intensities around the depth estimation point is required. At Porthtowan the spacing for the depth estimation points is 10 m in the crossshore direction and 25 m in the alongshore direction.

Depth estimation values are filtered in cBathy by allowing depths within a reasonable site specific depth range. For this application of cBathy the depth truncation is set to a minimum depth of 0.25 m and maximum depth of 20 m. Besides the depth truncation, a frequency range controls the depth estimations. Based on wave data a typical frequency range is determined. Considering the prevailing swell-dominated wave climate at Porthtowan, a range up to 18 seconds wave period is used. Δf was chosen as $100s^{-1}$ to create enough resolution around the longer wave periods.

The dimensions of the pixel sub-sampling domain are determined by the smoothing length scales. Smoothing takes place such that the contribution of the pixels to the final depth estimate is weighted through a Hanning filter. More weight is assigned to the pixels close to a depth analysis point when the sub-sampling domain is smaller while more spreading of the weighted contribution occurs if the sub-sampling domain is larger. The sub-sampling domain around the depth analysis point for Porthtowan has a width of Δx_m and a length of Δy_m (10 m and 25 m respectively).

2.4. Field data

Bed level data for ground truthing cBathy was collected in two ways. Following the work of Poate et al. (2009) in relation to the WAVEHUB (UK's wave energy array test site), monthly (inter-tidal) topographic surveys at Porthtowan have been carried out at spring low tide since 2008. Bathymetry measurements at neap tide have been periodically taken in addition to the topographic surveys since the application of cBathy at Porthtowan started (late 2012).

The monthly topography surveys are conducted using a GPS receiver mounted on an all-terrain vehicle(ATV) using real time kinematic (RTK) Global Positioning System (GPS). Alongshore lines are followed by the ATVdriver with a cross-shore spacing of between 7 and 10 m. Every metre or every second (depending on which occurs first) the GPS receiver stores a XYZ point in OSGB36 coordinates with an accuracy of O(5cm). Two bathymetry surveys have been conducted with a single beam echo-sounder on a small rigid-hull inflatable boat (RIB) or inflatable rescue boat (IRB). The echo-sounder estimates a depth by using the principle of measuring the double way transit time of an acoustic signal reflected by the seabed. A RTK-GPS receiver is mounted on top of the echo-sounder in order to couple the depth estimate with a real-world position and elevation in OSGB36 coordinates. The elevation together with the depth gives the bed level elevation. Both, topography and bathymetry are combined into one dataset and the data is subsequently interpolated on a grid using a local regression (LOESs) model (Plant et al., 2008).

Figure 2b shows a final result of the combined topographic and bathymetric data. For the following analysis, e.g. to determine RMS errors on a regional basis, we consider three areas in the bathymetric domain. The inter-tidal area (blue lines in Figure 2b) is the area where the quad bike surveys are carried out. In the sub-tidal zone an area around the sub-tidal bars (yellow lines in Figure 2b) is distinguished stretching from its boundary with the inter-tidal domain to well beyond the offshore extent of the bar. Further offshore of the bar an offshore region is defined (red lines in Figure 2b).

The one bathymetric survey used in this work was conducted during relatively calm wave conditions and during neap tide on the 10th of April, as presented in Table 2. Since the aim is to investigate the impact under macro-tidal conditions we assume that limited morphological change took place between the neap tidal survey and the next spring tide (17 April 2014). A comparison between the survey (Figure 2b), a depth estimate with cBathy on the survey day and an estimate with cBathy during the next spring tide is presented in section 3 and provides a picture of the behaviour of cBathy estimates under varying tidal ranges. Holman et al. (2013) shows that the accuracy of the depth estimates during mild wave conditions is typically distinguishably better than when more energetic wave conditions occur. Taking this into account, and considering the wave conditions during the bathymetric survey (Table 2 - 10 April 2014), one would expect that cBathy would work well for the day of bathymetric measurements (10 April 2014) and even better for the lower wave conditions experienced during the next spring tide (17 April 2014).

3. Results

3.1. Performance under macro tidal conditions

A bathymetry is estimated for all available hourly stack collections collected during daylight using the unmodified version of cBathy as presented in Holman et al. (2013). These hourly bathymetries (in the order of 12 per day around 10th of April) are combined into one bathymetry for the whole day through the Kalman filter. These filtered bathymetries are subsequently used for comparison with the bathymetric survey. Figure 3a shows the bathymetry estimates for the 10th of April (neap tide and survey day), and results for the 17th of April (spring tide) are presented in Figure 3b. The coast is in the upper part of the figures and offshore corresponds to the higher values along the X-axis (as Figure 2b). Similar features at corresponding locations are observed in the bathymetric survey (Figure 2b) and the estimate on the survey day (Figure 3a,b), for example, the sub-tidal bar at approximately 700 m crossshore position in the survey can also be found in the depth estimate and the trough at the onshore side of the sub-tidal bar shows a similar shape. In contrast to this performance are the estimates during the next spring tide (17th of April). The shape of a bar in both estimates is recognisable but it seems that the bar shape is more smeared out in the crossshore direction over the complete alongshore domain.

The difference between the bathymetry survey which was collected on 10 April 2014 and the cBathy depth estimates calculated for 10 April 2014 and 17 April 2014 are presented in Figures 3c and 3d respectively. The 17^{th} represents spring tide conditions. Although only a single realisation is presented here, a considerable difference in accuracy exists for the neap and spring tide depth estimation. Over most of the domain values of ± 3 m are found during the spring tidal depth estimate while for the neap tidal depth estimate the difference is more in the order of ± 1.5 m. Both difference plots show that cBathy underestimates the depth in most of the domain except for the shallowest parts of the domain. Holman et al. (2013) relates this overestimation of depth in shallow water to wave non-linearity due to breaking and hence poor correspondence with the linear dispersion relation in the surf zones. Tests including non-linear models have been carried out (Rutten, 2014) but significant improvements in estimating the depth in the shallower waters have not yet been achieved. Wave-induced currents to due wave breaking are a recognised source of error in the surfzone since the linear dispersion relation without currents is applied. Furthermore, Tissier et al.

(2015) showed that the short-wave celerity depends largely on infragravity modulations (infragravity wave height and induced velocity) in the surf zone. However, depth estimations are found not to be significantly more accurate when these infragravity modulations are accounted for. Closer to shore, when the waves break, the linear dispersion relation does not relate to the more bore-like wave physics. The technique observes a rather coherent and relatively fast moving structure, this results in significant overestimation of the depth. Also, one can argue that the inter-tidal zone does not experience as much wet-time as the deeper areas. This means that the final estimates using the Kalman filter will be constructed with less depth estimates.

Two representative crossshore profiles, at respectively 100 m and 300 m alongshore, are presented for both dates in Figure 3e,f. The estimate during neap tide on the 10th of April (Figure 3e) shows a significant underestimation of the depth over the bar (at 700 m crossshore) in both cross sections (100 and 300 m). An underestimation of the depth is also observed over the sand bar at Duck, NC (Holman et al., 2013). However, the sandbar at Duck is smaller and less pronounced than the sand bar at Porthtowan. Similar ground truth tests have been carried out at Egmond aan Zee in the Netherlands (Sembiring, pers. comm.). The comparison between a survey and cBathy estimates at Egmond shows a similar pattern to those from Porthtowan - an underestimation of the depth over the sand bar followed by an overestimation of the depth at the bar trough. Figure 3f shows the cross section during the next spring tide. The cross sections for the spring tidal estimate show that most of the domain experiences a significant underestimation of the depth. However, features are in approximately the right places but with a significant vertical offset. Differences between the survey and estimates up to 4.5 m can be found.

A Root-Mean-Square error was determined over the whole domain and per sub-domain (as indicated in Figure 2b) for the neap and spring-tide estimates and presented in Table 3. Over the whole domain this analysis reveals an RMS-error that is almost doubled during the spring-tide (2.05 m) compared to the neap tide (1.06 m). Around the sub-tidal bar region the most accurate estimates (RMS-error of 0.77 m) can be found. However, for the same region during spring tide the RMS error increases to 2.03 m. The dramatic increases in RMS-errors in all the domains suggests that the tide related accuracy is clearly a factor and directly relates to the accuracy of cBathy. Especially taking into account the expected higher accuracy concerning the smaller waves during the spring tide estimates (larger waves = larger bias (Holman et al., 2013)).

An increase in RMS-error with tidal range is not only found during the test case above but it is observed consistently. Although many additional factors can play a role (for example, wave height and water on the camera lens), a systematic increase of the RMS-error over the whole domain with tidal range (TR) is found at Porthtowan as indicated in Figure 4. For the lower tidal ranges (2 m$< TR <$ 4 m) a large spread of the RMS-error is found. One of the reasons for this is that wave heights up to 4 m were measured in the days before the survey. Larger waves show, in general, less accurate results with cBathy (Holman et al., 2013). For the larger tidal ranges ($TR >$ 4 m) the wave climate was relatively calm which results in a smaller range in RMS-error. Taking the context into account a slight trend of an increasing bias with increasing tidal range is observed.

3.2. Inaccuracies on camera boundaries

On the camera boundaries consistent inaccuracies in the depth estimates are found. The magnitude of this bias varies under different conditions. Although the bias varies in magnitude, the depth is consistently overestimated on the camera boundaries as shown in Figure 5a,b which shows the final, single estimate (5a) and the Kalman-filtered(5b), depth estimation. For individual estimates (the whole domain at a single point in time) this camera boundary effect can be rather large O(1 m). However, the combination of numerous estimates in the Kalman filter process tends to smooth the effect. This can be observed in Figure 5b, most of the domain experiences an underestimation but over most of the camera boundaries an overestimation is visible. As the distance from the camera system increases the impact of the camera boundary issue increases.

3.3. Modifications

From the results above the two suspected issues are confirmed; 1) inaccurate depth estimation on the camera boundaries and 2) a significant tide dependent inaccuracy. The differences between survey and depth estimates are up to 3 m and in the same order of magnitude as the measured local depth. Considering the difference in RMS-error between the neap and spring tide estimates we can confidently state that the tidal elevation plays an important role in the accuracy of the depth estimates. In the following two sections, respective solutions for the camera boundary and tide dependent discrepancies are presented.

3.3.1. Camera boundary solution [cB]

Higher inaccuracies around the camera boundaries are identified when cBathy is compared to the surveys (e.g. see Figure 5a,b). Such inter-camera differences are found at most of the sites where cBathy is applied [Duck (USA), Egmond aan Zee and the ZandMotor (Netherlands)]. A common work-around is to increase the spatial smoothing by enlarging the sub-sampling domain (Sembiring, pers com). Another approach seeks to derive perfect camera-geometries by adjusting individual camera geometry parametres in order to stitch the camera views perfectly together (Stanley, pers com). However, such approaches may not provide sufficiently accurate resolution or be practical, and so there is not yet a consensus about how to effectively overcome inaccuracies on the camera boundaries.

It is likely that even small errors in camera geometry solutions could lead to a significant difference between the estimated and real-world position of pixels. Such differences would result in a mismatch between the estimated phases across the camera boundary. Where the sub-sampling domain solely contains pixels from a single camera, depth is estimated independently from this phase shift, meaning that only wave number k and wave angle α are used from equation 3. However, on the camera boundary, where the sub-sampling domain contains pixels from multiple cameras, the fitting procedure of a single wave phase is unable to incorporate a sudden apparent shift in the phase over the sub-samples. Nevertheless, the fitting procedure will seek to find the best fitting solution which in most cases means that the wave angle is increased. When the wave angle is larger, the estimated wavelength is larger and so the resulting wave number k is smaller than it should be. Using this underestimated wave number in the linear dispersion relation then leads to an overestimation of the depth.

A new and effective solution to overcome this issue is presented here. If the sub-sampling domain contains pixels from multiple cameras the processing system automatically splits the depth estimation procedure into separate but parallel processes in which only pixels from single cameras are used. In this way any potential difference in phase is removed (Equation 3) as intended and only the wave number and wave angle are used. However, with this method, two wave numbers and two wave angles are found for the sub-sampling domain while only one depth estimate is desired. To counter this, the two separate depth estimates are combined through a weighted average based on the location of their centre of mass relative to the required location of the depth estimate. An accuracy measure is not incorporated in the weighting as the normal quality control within the cBathy routines determines whether a depth estimate is reliable or not. Figure 6 illustrates the significant improvement that is achieved when the camera boundary solution is applied. Figure 6a represents the bathymetry estimation without the camera solution. A clear overestimation of the depth on the camera boundaries is found between camera 2 and 3. Figure 6b shows a depth estimation with the camera boundary solution implemented. Improved depth estimations on the camera boundaries are the result and, the camera boundary issue is no longer apparent.

3.3.2. Tide dependent floating pixels [TPix]

A significant variation in performance of cBathy with the tidal range is a consequence of the limited inclusion of tidal elevation in the code which results in fixed geographical pixel locations. The only use of tidal elevation is to transform depth estimates to an absolute reference level. Geographical pixel locations are determined once only when data collection is initially scheduled. However, the reference level, and hence the set of geographical pixel locations, changes as the water level rises and lowers with the tide. A set of pixels moves towards the camera system, and at the same time the spatial footprint of the set contracts, during a rising tide, while during a falling tide the opposite occurs, with pixels moving further from the camera and relative expansion of the pixel set footprint. Figure 7 presents this process schematically, where the orange squares represent the pixel domain in the current version of cBathy and the blue and green squares represent the reality for low and high tide respectively. Incorrect pixel positions result in a shorter sensed wavelength than in reality at low tide which leads to an overestimation of the wave number and thus an underestimation of the depth, and vice versa for high tide.

The pixel shifting is not solely dependent on the tidal elevation but, rather, is a function of tidal elevation, vertical position of the camera system and distance to the camera. The maximum shift as a percentage of the distance between pixel and camera system can be found with the ratio TR_{max}/z_{cam} where TR_{max} is the maximum tidal range and z_{cam} is the vertical position of the camera system. The instantaneous pixel shifting can be calculated using Equation 5.

$$(dx\left(t\right), dy\left(t\right)) = \frac{\eta_{tide}\left(t\right)}{z_{cam}}\left(x_{ref} - x_{cam}, y_{ref} - y_{cam}\right) \tag{5}$$

Where dx, dy represent the shift in respectively x and y direction, η_{tide}

relates to the tidal elevation, z_{cam} is the camera height and the subscripts ref and cam refer respectively to the reference and camera position for x and y. For Porthtowan, a ratio of 15.9% is found using z_{cam} = 44 m and a TR_{max} = 7 m. This means that with a camera reach of around 1880 m in the far end of the domain the pixels move around 300 m back and forth between low and high spring tide. The horizontal shift of the pixel location is +/- half the total shift since the excursion that should be accounted for starts at the initial pixel location obtained using the vertical reference level (mid-tide at Porthtowan, $z = 0$ m). To overcome this issue an additional inclusion of the tide in the code was implemented following Equation 5. For every stack collection the pixel location is recalculated according to the tidal elevation.

3.4. Performance with modifications

Bathymetry estimates for neap (left) and spring (right) tide including the floating pixels and camera boundary solution are presented in Figure 8a-d. Unlike the estimates with the original version of cBathy (Figure 3), estimates with the modifications show corresponding bar features in both spring and neap tidal estimates. Features like a rip channel (X = 600 m, Y = 0 m) and the sub-tidal bar are better resolved compared to the original version which indicates a clear improvement in performance. Inaccurate depth estimates are still found in the very shallow parts of the domain but as mentioned before this is likely due to the invalidity of the linear dispersion relation for that area.

Table 4 shows the calculated Root Mean Square (RMS) error and its percentage of the measured depth per step in the modifications for the whole domain and the specific regions indicated earlier in Figure 2b. Considering the whole domain, a reduction of 8.5% with exclusively the floating pixel solution is found. If the floating pixel and camera boundary solution are applied simultaneously the RMS error is reduced by up to 19%. For the next spring tide a larger reduction is found with solely the floating pixel solution (49%). The combination of the floating pixels and camera boundary solution results in almost 53% reduction of RMS error. The improvement in accuracy was greatest for the sub-tidal bar area shifting from 2.03 m RMS error to 0.49 m. The RMS error as a percentage of the depth reduced in the sub-tidal bar region from 39% to 9%.

The overall RMS error is comparable (between 0.86 and 1.05 m) for all the new configurations. For the sub-tidal region a significant improvement is reached, the RMS error decreased from 2 m to 50 cm with the modifications. The difference between neap and spring tide depth estimates in the sub-tidal bar domain for the original version is 260%. When both the new camera boundary and floating pixel solutions are implemented simultaneously, the best performance occurs around the sub-tidal bar region (RMS-error of around 50 cm), around 9-10% of the local water depth.

4. Discussion

4.1. Improved performance at Porthtowan

The results, in particular Figure 8 and Table 4, show a significant improvement using the two modifications compared to the estimates without the modifications. However, the data shown only comprises a single survey campaign and it remains a question whether the accuracy of the depth estimates is consistently ameliorated. Figure 9 shows that an improvement in estimating depth is found when the modifications are applied to other arbitrary depth estimations around the time of the survey (Figure 2b).

Figures 9a and 9b show the RMS error over the whole domain against tidal range and wave height for the exact same points in time. Figure 9c shows the reduction in percentage of the RMS error between cBathy (Holman et al., 2013) (9a) and cBathy with both corrections (9b). Depths estimated with the original cBathy code at a tidal range larger than 4.5 m seem to coincide with RMS errors larger than 1.5 m. With the inclusion of the floating pixels and the camera boundary solution the same estimates have a RMS error lower than 1.5 m. Figure 9c shows that the largest improvement is achieved for the largest tidal ranges (as expected) during relatively calm wave conditions. At maximum, a reduction of 60% in RMS error over the whole domain is reached. The largest reductions in RMS error are found with limited wave heights (< 1 m).

The depth estimates shown in Figure 9 are representative for the day consisting of Kalman-filtered hourly depth estimates. Depending on the number of light hours per day, a certain amount of hourly depth estimates (maximum 16 hours during the longest day) are combined together for a daily estimate. With more data the Kalman filtered depth estimates perform better. Furthermore, if the Kalman filtering starts with a measured bathymetry it starts from a relative accurate starting point. The Kalman like filter will keep the measured depth until the faith in the depth value has diminished over time or the cBathy estimates have a greater Kalman gain factor.

4.2. Potential effects at other sites

The issue on the camera boundaries is observed at other sites, for example at a recently installed video station near to the Sand Engine in the Netherlands (Holman, pers com). The camera boundary solution in its current form shows that the principle of estimating wave numbers per camera and combining them afterwards works at Porthtowan. This solution is easily transferable to other cBathy sites and collected data can be re-analysed with the solution implemented. Nevertheless, the camera boundary solution could be extended by incorporating cBathy's quality measure concerning the wave phase fitting.

The reduction in bias of the depth estimation related to the floating pixel solution is site specific. Equation 5 suggests that tide-related inaccuracies in the cBathy depth estimates are not exclusively occurring at sites with a large tidal range. The vertical angle (ratio between tidal range and vertical camera position) is the key-factor and can potentially cause tide related inaccuracies in macro/meso tidal environments when the camera system is mounted relatively low. Figure 10 shows the pixel displacement (presented on logarithmic scale) in relation to tidal range and the ratio between the distance from the camera (d) and the camera height (h) for a range of sites. The greyed area in Figure 10 shows the pixel displacement for all the pixels considered at Porthtowan. The pixels farthest away from the camera experience almost $10^{2.5} = 316$ m displacement.

Pixel displacement information for some other sites where video camera systems are sited but with smaller tidal ranges is also presented in Figure 10. The chosen (most 'famous') Argus sites are Duck NC (USA), Palm

Beach (AUS) and Egmond aan Zee (NL) and non-Argus sites are Biscarrosse (FRA) (Almar et al., 2008; Sénéchal et al., 2009) and Alfeite (PT) (Silva et al., 2009). Although the tidal range at all the sites is significantly lower compared to Porthtowan, the total pixel displacement between low and high tide due to the tidal elevation is up to 80 m in the outer edge of the domain at Egmond aan Zee. If this is not taken into account this displacement would mean that pixels are used to estimate a depth that are not around the point of interest but 40 m further away from the camera (if the vertical reference level is mid-tide).

5. Conclusions

Video-based bathymetry estimations are obtained at Porthtowan using an inverse method following linear dispersion relation of free surface elevations. Two areas of inaccurate depth estimation are identified: 1) inaccurate depth estimation on the camera boundaries and 2) tide dependent bias in depth estimation due to the lack of the exact position of the pixels in cBathy. On the boundary, where the camera field of view are overlapping or bordering, imprecise sensing of the propagation of the wave due to various reasons such as differences in distortion and independent camera movement result in an apparent abrupt phase shift and lead to errors in the depth estimation. A straightforward solution to diminish the observed systematic overestimation of depth on the camera boundary is proposed. The depth estimation analysis is performed independently for each camera to overcome these inaccuracies. The second identified source of inaccuracy is the tide dependent inaccuracy. Here, the formerly fixed positions of the pixels in the real-world have been changed to floating pixel positions depending on the instant tidal elevation and the camera height. Floating pixels are not only important in macro-tidal environments, since the magnitude of this effect depends on the tidal range and camera height. The two modifications to the unmodified cBathy version as presented in Holman et al. (2013) lead to significant improvements over the whole domain at Porthtowan. Depending on multiple environmental variables, up to a 60% reduction in RMS-error over the whole domain (Figure 9) and 75% reduction in RMS error in the sub-tidal bar domain has been demonstrated (Table 4) here. The video camera system at Porthtowan, with the inclusion of the modifications, is then shown to be capable of estimating the sub-tidal depths with a bias of around 10% of the local depth.

6. Acknowledgement

This work is part of the PhD process of the first author. The PhD-project is funded by Quality Research/Research Excellence Framework CarePlan. The authors would like to thank Rob Holman for his comments on the work and especially the help to understand the cBathy coding and working in depth. We would like to thank Deltares for sharing the cBathy coding and implementation of stack collection at the Argus station in Porthtowan. The authors are thankful to all the help of members from the Coastal Processes Research Group during the different topography and bathymetry surveys, in particular Christopher Stokes and Sam Prodger. For the tidal elevation prediction and Kalman filter the offshore atmospheric pressure and wave data close to Porthtowan is used. The wave and atmospheric pressure data for the Perranporth wave buoy is courtesy of the South-West Regional Coastal

Monitoring Programme and is available on www.channelcoast.org/southwest. The authors would like to thank the reviewers for their detailed comments that have undoubtedly helped to improve the paper.

Aarninkhof, S. G., Ruessink, B. G., Roelvink, J. A., 2005. Nearshore subtidal bathymetry from time-exposure video images. Journal of geophysical Research vol. 110.

Aarninkhof, S. G., Turner, I. L., Dronkers, T. D., Caljouw, M., Nipius, L., Oct. 2003. A video-based technique for mapping intertidal beach bathymetry. Coastal Engineering 49 (4), 275–289.

Almar, R., Bonneton, P., Roelvink, N. S. D., 2008. Wave celerity from video imaging: A new method. In: Proceedings of the 31st International Conference Coastal Engineering. pp. –.

Austin, M. J., Scott, T. M., Russell, P. E., Masselink, G., 2013. Rip current prediction: Development, validation, and evaluation of an operational tool. Journal of Coastal Research vol. 29, 383–300.

Bell, P. S., 1999. Shallow water bathymetry derived from an analysis of x-band marine radar images of waves. Coastal 37, 513–527.

Bergsma, E. W. J., Conley, D. C., Davidson, M. A., O'Hare, T. J., Holman, R. A., 2014. An assesment of video-based bathymetry estimation in a macro-tidal environment. In: Lynett, P. J. (Ed.), Coastal Engineering, Proc. 34th Conference on Coastal Engineering. Vol. 34. Seoul.

Birrien, F., Castelle, B., Marieu, V., Dubarbier, B., 2013. On a data-model assimilation method to inverse wave-dominated beach bathymetry using hetrogeneous video-derived observations. Ocean Engineering.

Buscombe, D., Scott, T., 2008. Coastal geomorphology of north cornwall: St. ives to trevose head. internal report for wave hub impacts on seabed and shoreline processes. Tech. rep., University of Plymouth.

Castelle, B., Ruessink, B., Bonneton, P., Marieu, V., Bruneau, N., Price, T., 2010. Coupling mechanisms in double sandbar systems. part 1: Patterns and physical explanation. Earth Surface Processes and Landforms vol. 35, 476–486.

Catálan, P. A., Haller, M. C., 2008. Remote sensing of breaking wave phase speeds with application to non-linear depth inversions. Coastal Engineering vol 55, 93–111.

Chickadel, C. C., 2003. An optical technique for the measurement of long-shore currents. Journal of Geophysical Research 108 (C11), 3364.

Coco, G., Murray, A. B., 2007. Patterns in the sand: From forcing templates to self-organization. Geomorphology vol. 91, 271–290.

Coco, G., Senechal, N., Rejas, A., Bryan, K., Capo, S., Parisot, J., Brown, J., MacMahan, J., 2013. Beach response to a sequence of extreme storms. Geomorphology.

Davidson, M., van Koningsveld, M., de Kruif, A., Rawson, J., Holman, R., Lamberti, A., Medina, R., Kroon, A., Aarninkhof, S., 2007. The coastview project: Developing video-derived coastal state indicators in support of coastal zone management. Coastal Engineering vol. 54, 463*–475.

Guza, R. T., Thornton, E. R., Holman, R. A., 1984. Swash on steep and shallow beaches. In: Proceedings of the 9th International Conference on Coastal Engineering, edited by B.L. Edge.

Holland, T. K., 2001. Application of the linear dispersion relation with respect to depth inversion and remotely sensed imagery. Transactions on Geoscience and Remote Sensing.

Holman, R., Stanley, J., Jun. 2007. The history and technical capabilities of Argus. Coastal Engineering vol. 54 (6-7), 477–491.

Holman, R. A., Plant, N., Holland, T., 2013. cBathy: A Robust Algorithm For Estimating Nearshore Bathymetry. J. Geophys. Res. Oceans vol. 118.

Lippmann, T. C., Holman, R. A., 1990. The spatial and temporal variability of sand bar morphology. Journal of geophysical Research vol. 95, 11575–11590.

Masselink, G., Scott, T., Poate, T., Russell, P., Davidson, M., Conley, D., 2015. The extreme 2013/2014 winter storms: hydrodynamic forcing and coastal response along the southwest coast of england. Earth Surface Processes and Landforms vol.

Misra, S. K., Kennedy, A. B., Kirby, J. T., 2003. An approach to determining nearshore bathymetry using remotely sensed ocean surface dynamics. Coastal Engineering vol. 47, 265–293.

Plant, N. G., Holland, K. T., Haller, M. C., 2008. Ocean Wavenumber Estimation From Wave-Resolving Time Series Imagery. IEEE Transactions on Geosciences and Remote Sensing 46, 2644–2658.

Plant, N. G., Holman, R. A., 1997. Intertidal beach profile estimation using video images. Marine Geology vol. 140, 1–24.

Poate, T., Kingston, K., Masselink, G., Russell, P. E., 2009. Response of high-energy, macrotidal beaches to seasonal changes in wave conditions: Examples from north cornwall, uk. Journal of Coastal Research, SI 56 (Proceedings of the 10th International Coastal Symposium) 56, 747–751.

Poate, T., Masselink, G., Russell, P., Austin, M., 2014. Morphodynamic variability of high-energy macrotidal beaches, cornwall, uk. Marine Geology vol. 350, 97–111.

Rutten, J., 2014. Depth inversion including non-linear wave celerity, argus Workshop, September 2014.

Sénéchal, N., Gouriou, T., Castelle, B., Parisot, J.-P., Capo, S., Bujan, S., Howa, H., 2009. Morphodynamic response of a meso- to macro-tidal intermediate beach based on a long-term data set. Geomorphology vol. 107, 263–274.

Silva, A., Taborda, R., Catalão, J., Freire, P., 2009. Dtm extraction using video-monitoring techniques: Application to a fetch limited beach. In: Proceedings of the 10th International Coastal Symposium. pp. 203–207.

Smit, M., Reiniers, A., Ruessink, G., Roelvink, D., 2008. The mophological response of a nearshore double sandbar system to constant wave forcing. Coastal Engineering vol. 55, 761–770.

Stockdon, H. F., Holman, R. A., 2000. Estimation of wave phase speed and nearshore bathymetry from video imagery. Journal of geophysical Research vol. 105, 22015–22033.

Tissier, M., Bonneton, P., Michallet, H., Ruessink, G., 2015. Infragravity-wave modulation of short-wave celerity in the surf zone. Journal of Geophysical Research.

van Dongeren, A., Plant, N., Cohen, A., Roelvink, D., Haller, M. C., Catalán, P., Dec. 2008. Beach Wizard: Nearshore bathymetry estimation through assimilation of model computations and remote observations. Coastal Engineering 55 (12), 1016–1027.

Wallace, J. M., Dickinson, R. E., 1972. Empirical orthtogonal representation of time series in the frequency domain. part i: Theoretical considerations. Journal of Applied Meteorology vol. 11, 887–892.

Williams, W. W., 1946. The determineation of gradients on enemy-held beaches. The Geographical Journal vol. 109, 76–90.

Wilson, G., Özkan-Haller, H., Holman, R., 2010. Data assimilation and bathymetric inversion in a two-dimensional horizontal surf zone model. Journal of Geophysical Research.

Wilson, G., Özkan-Haller, H., Holman, R., Haller, M., Honegger, D., Chickadel, C., 2014. Surf zone bathymetry and circulation predictions via data assimilation of remote sensing observations. Journal of Geophysical Research: Oceans.

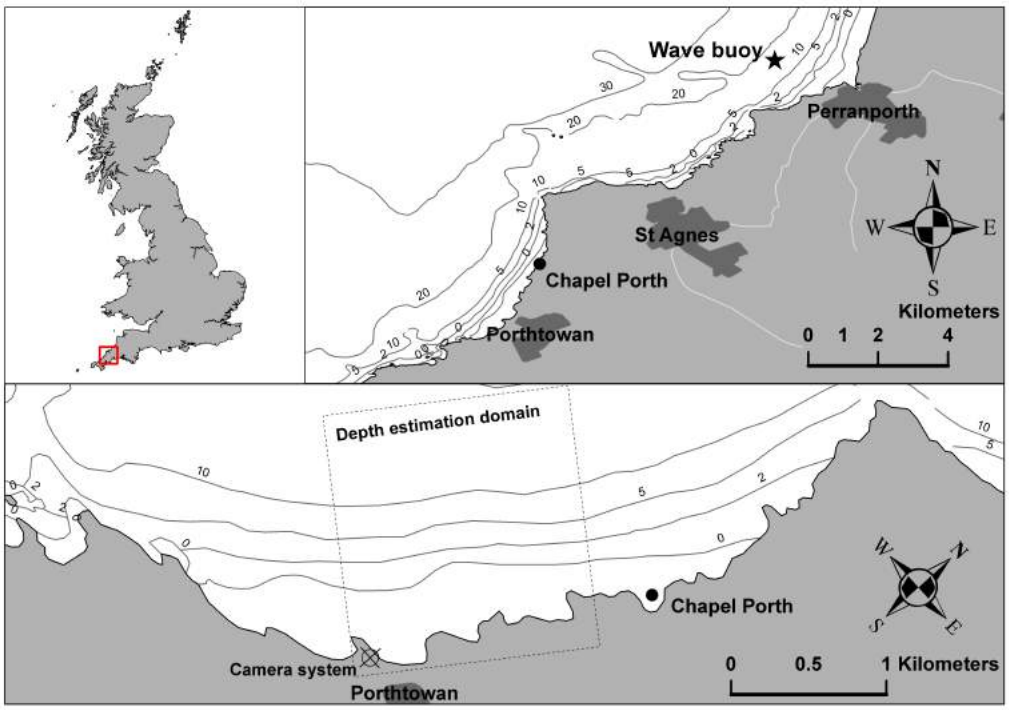

Figure 1: Map showing the study site (Porthtowan) in the South-West of England, Chapel Porth being the Northern boundary of the study site and the wave buoy at Perranporth. The lower panel shows a close up on the bay in the vicinity of Porthtowan.

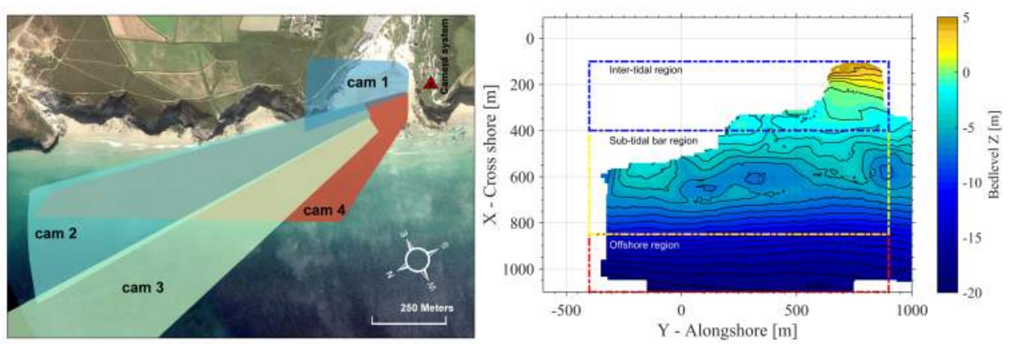

(a) (b)

Figure 2: a) Camera layout at Porthtowan, four cameras are located on the Southern cliff looking Northwards alongshore. b) Measured bathymetry (10 April 2014) with the overlaying lines indicate the different regions for the further analysis; inter-tidal (blue), sub-tidal bar region (yellow) and offshore region (red).

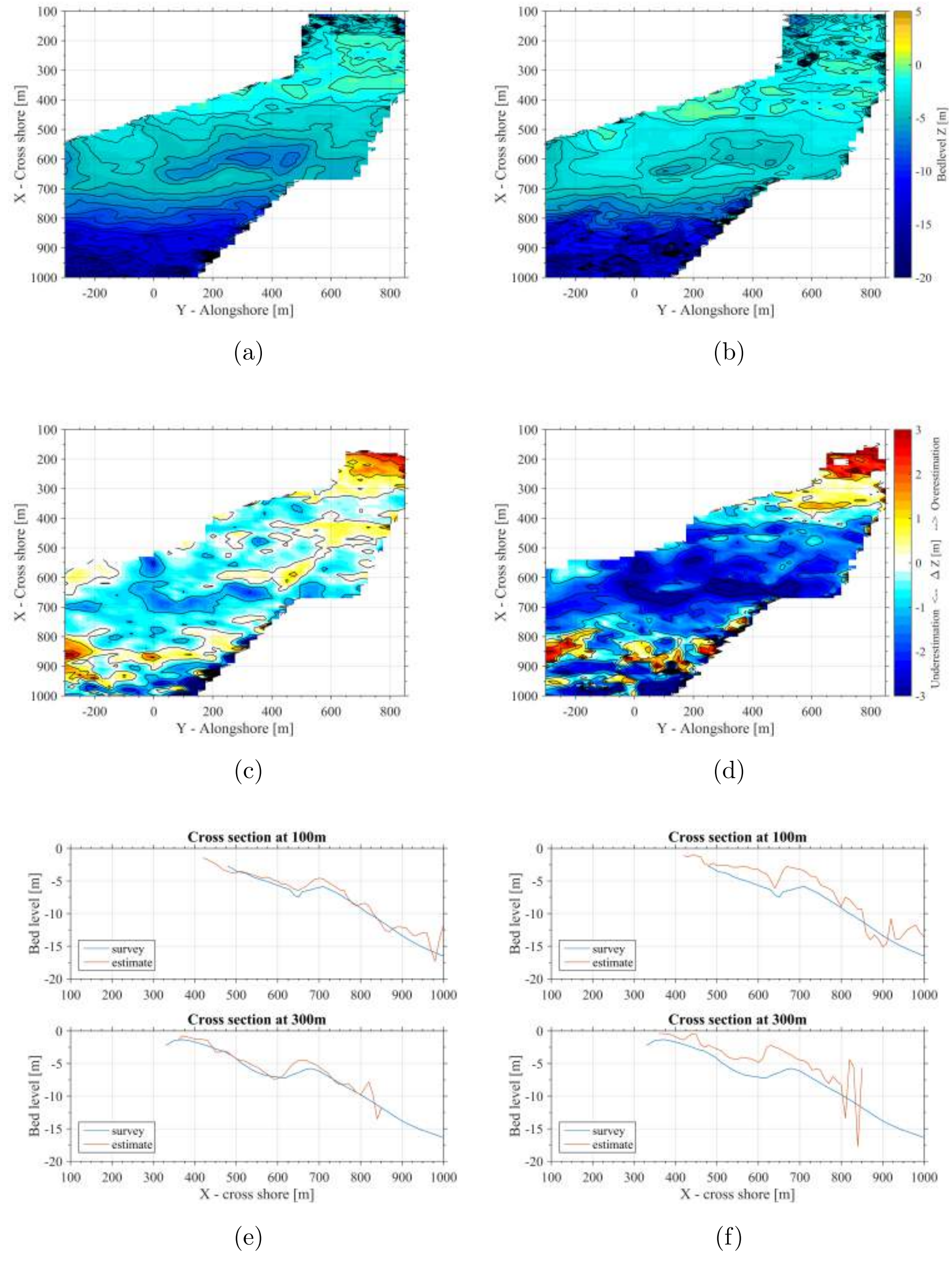

Figure 3: On the left side respectively the bathymetry estimate on the 10th of April 2014 (a), the difference to the survey (c) and two cross sections (e) (at 100m and 300m) are shown. On the right side respectively the bathymetry estimate (b), the difference to the survey (d) and two cross sections (f) (at 100m and 300m) on 17 April 2014 are presented.

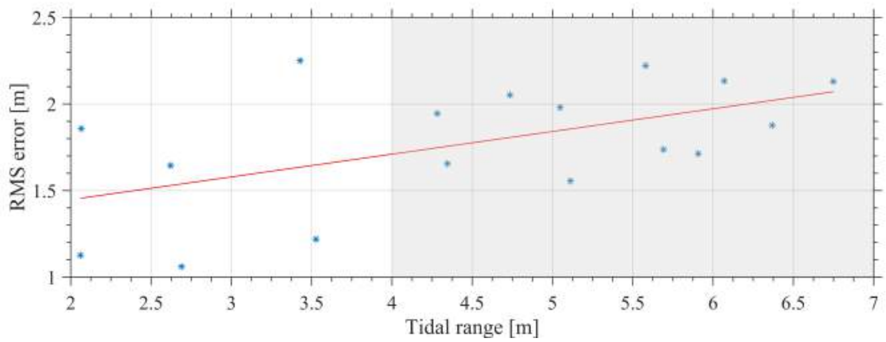

Figure 4: RMS error compared to wave height and tidal range. Red line represents a linear regression with $r^2 = 0.295$ and is significant ($p = 0.024$) at the 95% confidence interval. Grey patch indicates the domain of the macro tidal range ($TR > 4$).

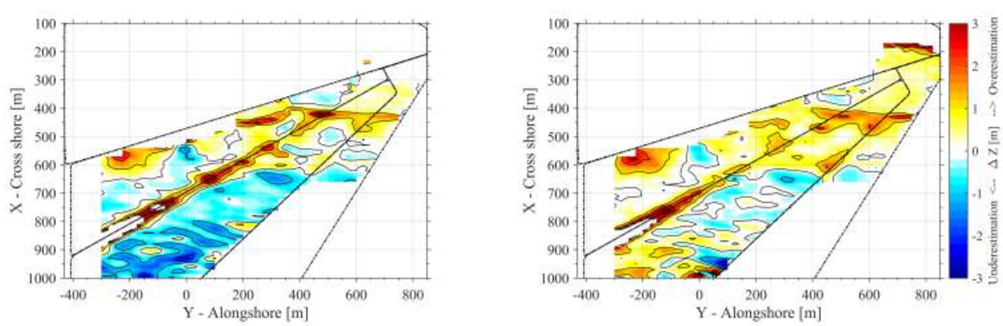

(a) (b)

Figure 5: Difference between the survey (10 April 2014) and estimates (9 April 2014). (a) represents the difference between the survey and a single estimate (18:00) and (b) is the difference between the survey and the daily Kalman filtered result. The black lines represent the camera boundaries.

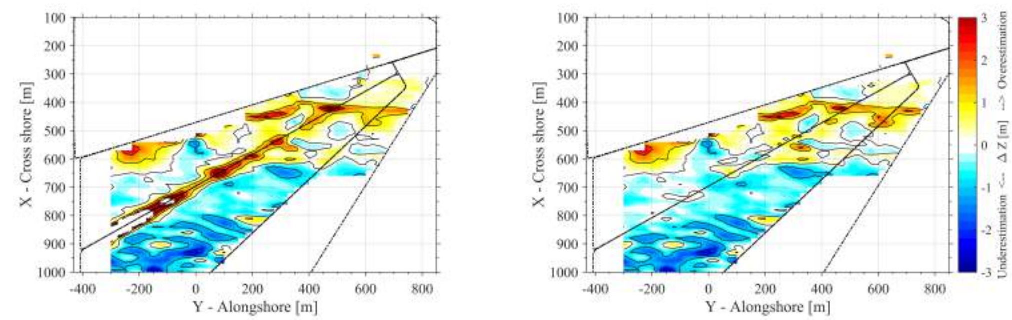

(a) (b)

Figure 6: Difference between the survey (10 April 2014) and estimates (9 April 2014). (a) represents the difference between the survey and a single estimate (18:00) without the solution and (b) shows the difference between the survey and the same single estimate (18:00) with the camera boundary solution. The black lines represent the camera boundaries.

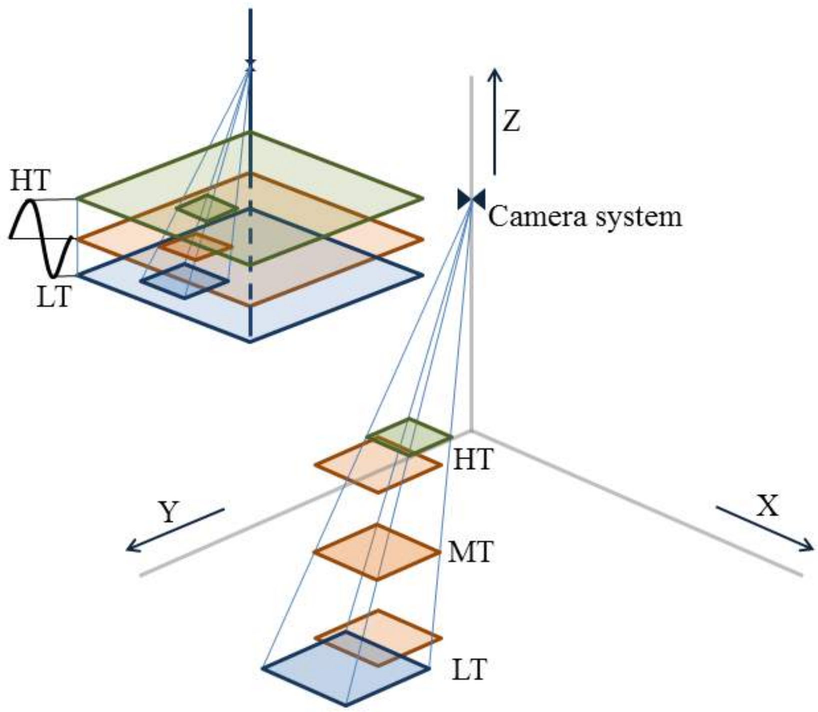

Figure 7: The squares represent a selection of pixels moving up and down with the tidal elevation. The pixel set moves respectively towards the camera system and away from it. At the same time relative contraction and expansion between the pixels takes place

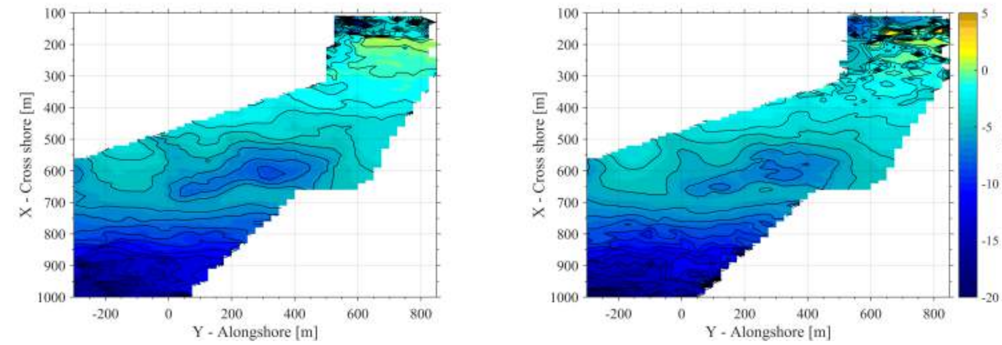

(a) (b)

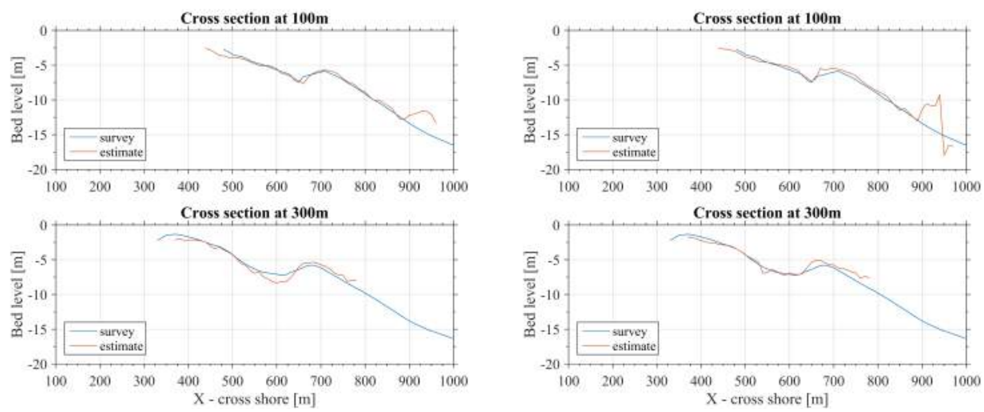

(c) (d)

Figure 8: On the left panel respectively a renewed bathymetry estimate using the modifications on the 10th of April 2014 (a) and two cross sections (c) at X=100 m and X=300 m. On the right is the renewed bathymetry estimate (b) on 17 April 2014 and the corresponding cross sections (d) at X=100 and X=300

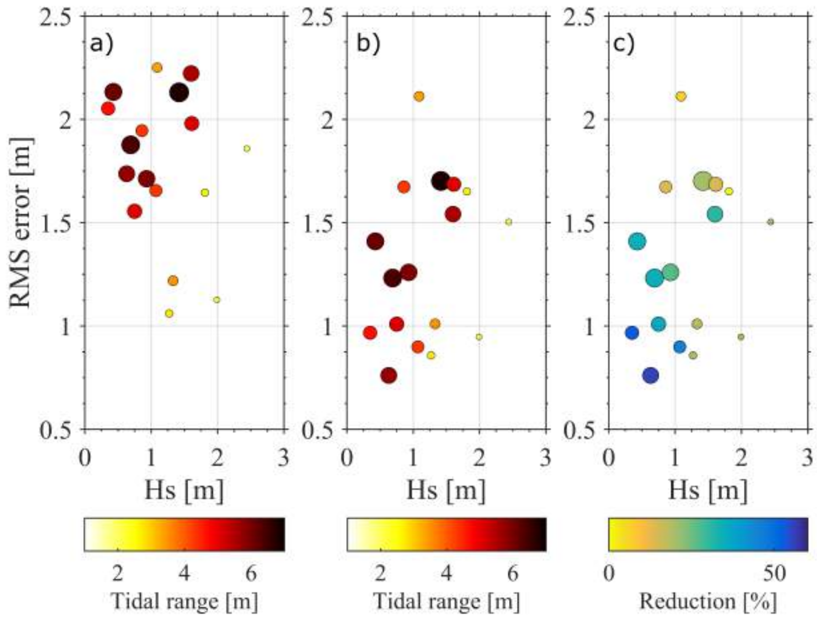

Figure 9: RMS error versus significant wave height [Hs] over the whole domain where the marker size represents the tidal range at the time of the depth estimation. For the left and middle panel the colour corresponds to the tidal range while for the right panel the reduction of RMS-error in percentage is represented by the colour. The left panel represents the RMS error for cBathy as presented in (Holman et al., 2013), the middle panel shows the RMS error for cBathy with the floating pixel and camera boundary solutions together and the right panel shows the percentage reduction of the RMS error.

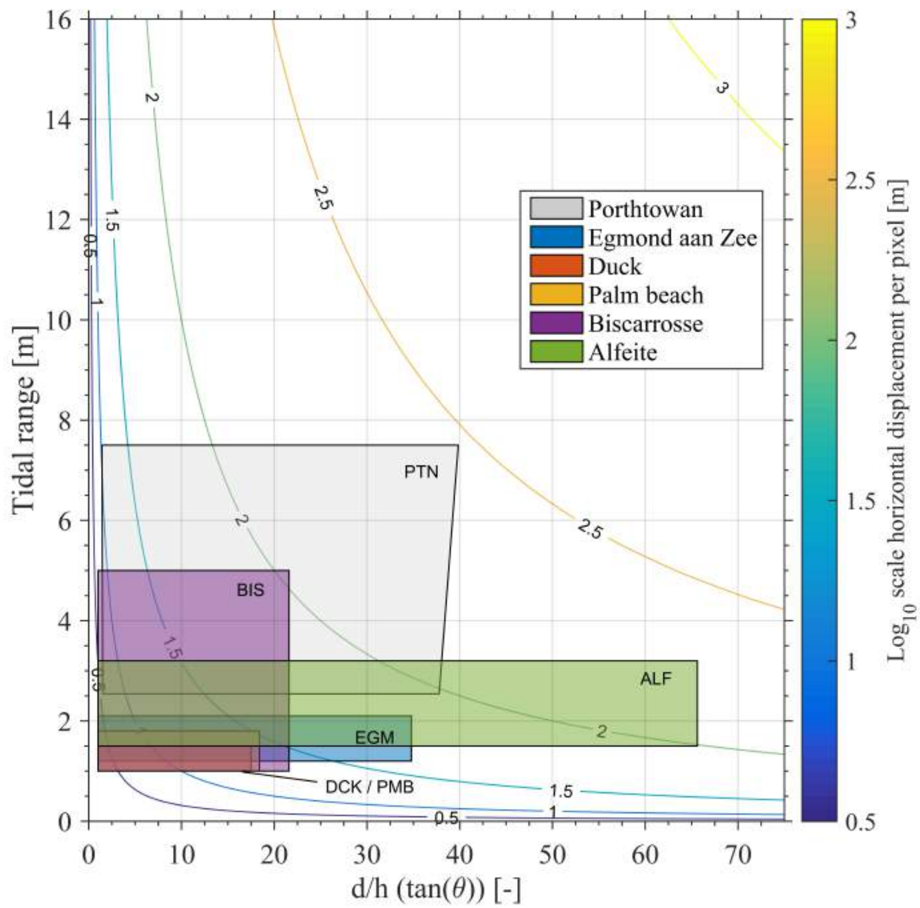

Figure 10: Horizontal pixel displacement (log scale) as function of the tidal range and ratio d/h (d = distance from the camera and h = camera height)

Description	value(s)	units
Pixel collection spacing (Δx_p)	4.0	m
Pixel collection spacing (Δy_p)	10.0	m
Depth analysis spacing (Δx_m)	10.0	m
Depth analysis spacing (Δy_m)	25.0	m
Allowable depth range [h_{min} to h_{max}]	0.25 to 20.0	m
Frequency domain [f_{min} to f_{max}]	1/18 to 1/4	1/s
Δf	1/100	1/s
Smoothing scales (in depth analysis)	Δx_m, Δy_m	

Table 1: Overview of Porthtowan specific settings for cBathy

	TR$_{max}$ [m]	Hs [m]	Tp [sec]	Dir [°]
10 April 2014	2.78	1.16	10.51	278.4
17 April 2014	6.03	0.52	10.38	278.9

Table 2: Tide range and day-average wave conditions for the two estimate examples used here. The survey for this work has been carried out on the **10th of April 2014**.

RMS error →	All [m]	inter-tidal [m]	sub-tidal [m]	sub-tidal Bar [m]	Offshore [m]
10 April 2014	1.06	1.15 (350%)	1.05 (14%)	0.77 (14%)	1.84 (13%)
17 April 2014	2.05	1.77 (623%)	2.12 (36%)	2.03 (39%)	2.43 (17%)

Table 3: The RMS errors are displayed here for cBathy (Holman et al., 2013). Results show the whole domain (All) and per area (inter-tidal, sub-tidal, sub-tidal bar and offshore) on the survey day (10 April 2014) and next spring-tide (17 April 2014). In brackets is the RMS error as percentage of the measured depth (mean over the (sub)domain).

RMS error →	All [m]	inter-tidal [m]	sub-tidal [m]	sub-tidal Bar [m]	Offshore [m]
10 April 2014 [cBathy]	1.06	1.15 (350%)	1.05 (14%)	0.77 (14%)	1.84 (13%)
17 April 2014 [cBathy]	2.05	1.77 (623%)	2.12 (36%)	2.03 (39%)	2.43 (17%)
10 April 2014 [TPix]	0.97	0.98 (160%)	0.97 (13%)	0.73 (14%)	1.70 (12%)
17 April 2014 [TPix]	1.05	1.63 (610%)	0.90 (11%)	0.59 (10%)	1.74 (12%)
10 April 2014 [TPixcB]	0.86	0.99 (160%)	0.83 (10%)	0.55 (9%)	1.59 (11%)
17 April 2014 [TPixcB]	0.97	1.51 (600%)	0.84 (10%)	0.49 (9%)	1.70 (12%)

Table 4: The RMS errors are displayed here for cBathy (Holman et al., 2013) [Orig], cBathy with the floating pixel solution [TPix] and cBathy with the floating pixel and camera boundary solution [TPixcB]. Results show the whole domain (All) and per area (inter-tidal, sub-tidal, sub-tidal bar and offshore) on the survey day (10 April 2014) and next spring-tide (17 April 2014). In brackets is the RMS error as percentage of the measured depth (mean over the (sub)domain).